# Dalton Transactions

ROYAL SOCIETY OF CHEMISTRY

## ARTICLE

# Eight coordinated mononuclear dysprosium complexes of heptadentate aminophenol ligands: the influence of the phenol substituents and the ancillary donors on the magnetic relaxation

Matilde Fondo,[a,*] Julio Corredoira-Vázquez,[a] Ana M. García-Deibe,[a] Jesús Sanmartín-Matalobos,[a] Daniel Reta,[b] and Enrique Colacio[c]

The mononuclear complexes [Dy(3Br,5Cl-H₃L$^{1,1,4}$)(D)]·solvate (D = H₂O, solvate = 0.25MeOH, **1W**·0.25MeOH; D = Py without solvate, **1Py**), and [Dy(3NO₂,5Br-H₃L$^{1,1,4}$)(H₂O)] (**2W**) were isolated. The crystal structures of **1W**·0.25MeOH, **1Py** and **2W**·2CH₃C₆H₅ show that the Dy$^{III}$ ion is octacoordinated, in $N_4O_4$ or $N_5O_3$ environments, with distorted geometries, between square antiprism, biaugmented trigonal prism and triangular dodecahedral. A similar environment for the metal ion is shown in the chiral crystals of the diamagnetic yttrium analogue [Y(3Br,5Cl-H₃L$^{1,1,4}$)(MeOH)] (**3M**), which were spontaneously resolved. Magnetic analyses of the three dysprosium complexes, and its diluted analogous **1W@Y**, **1Py@Y** and **2W@Y**, reveal that none of them seem to relax through an Orbach mechanism in $H_{dc}$ = 0. However, the three complexes show Orbach relaxation under $H_{dc}$ = 1000 Oe, and **1Py** is the in-field SIM with highest energy barrier among these complexes, with an $U_{eff}$ value of 358 K. Analysis of ac magnetic data shows that the electron-withdrawing substituents on the phenol rings of the aminophenol ligands, as well as the auxiliary oxygen donors from water ligands, reduce the energy barriers of the complexes, which is attributed to a charge reduction in the coordinating atoms of the aminophenol donor. *Ab initio* calculations support the experimental results.

## Introduction

Single ion magnets (SIMs) are a field of increasing importance within the study of molecular magnets. This is because anisotropy is known to be the driving force behind the enhancement of magnetic properties, as exemplified by a steady increased of the reported blocking temperature ($T_B$),[1-6] and this parameter is easier to control in mononuclear than in polynuclear complexes. Thus, the charge distribution about the central ion is one of the key factors to enhance the magnetic anisotropy, and, therefore, to achieve high performance SIMs.[1] Currently, the search for SIMs with increasing blocking temperatures is primarily focused on the two families of compounds that have reached the highest energy barriers and blocking temperatures: the pseudo-linear dysprosium biscyclopentadienyl family,[7-9] with record $T_B$ = 80 K,[9] and the pentagonal bipyramidal (pbp) dysprosium compounds,[10-17] with record hysteresis temperature of 30 K.[16] Nevertheless, all reported metallocenes are unstable in air. In the same way, only a small

number of the pbp dysprosium complexes with high blocking temperature were isolated in air.[10,12,13,16] Accordingly, much research is being done in the field, in an attempt to obtain high performance air stable SIMs. In this way, recently, an air stable dysprosium complex with square antiprism geometry was reported to show an energy barrier of 944 K under zero field.[18] Although square antiprism Dy$^{III}$-SIMs hardly ever show comparatively competitive properties, this reported study[18] shows that there exist alternative strategies to pseudolinear and pbp geometries that can give rise to improved SIM characteristics.

With the above considerations in mind, as a part of our study on the magnetic properties of complexes with polydentate ligands,[19-21] we decided to investigate the chemistry of dysprosium with a family of air stable heptadentate aminophenol flexible ligands, bearing a $N_4O_3$ set of donor atoms. This kind of donor has demonstrated that can yield mononuclear pbp Yb complexes,[20,22] or dinuclear phenoxide-bridged dysprosium and holmium compounds, with distorted triangular dodecahedral geometry and promising magnetic properties.[21] However, the reactivity of this type of ligand toward lanthanoids is still poorly studied. Thus, in this paper we report three new mononuclear Dy$^{III}$ compounds with two new different $N_4O_3$ donors, and their magnetic analysis, which allows studying the influence of both the auxiliary donors and the substituents of the aromatic phenol rings on the magnetic behaviour.

*a Departamento de Química Inorgánica, Facultade de Química, Universidade de Santiago de Compostela, 15782 Santiago de Compostela, Spain*
*E-mail: matilde.fondo@usc.es.*
*b Departament de Química Inorgànica i Orgànica, Facultat de Química, Universitat de Barcelona, 08028 Barcelona, Spain*
*c Departamento de Química Inorgánica, Facultad de Ciencias, Universidad de Granada, 18071 Granada, Spain*

# Experimental

## Materials and general methods

All chemical reagents were purchased from commercial sources, and used as received without further purification. Elemental analyses of C, H and N were performed on a Themoscientific Flash Smart analyser. Infrared spectra were recorded in the ATR mode on a Varian 670 FT/IR spectrophotometer in the range 4000-500 $cm^{-1}$. ^{1}H NMR spectra were recorded on a Varian Inova 400 spectrometer. Micro X-ray fluorescence quantitative analyses of Y and Dy for **1W**@Y, **1Py**@Y and **2W**@Y were recorded on a Bruker TORNADO 4 device.

## Syntheses of the ligands

The aminophenol ligands 3Br,5Cl-$H_6L^{1,1,4}$ and 3NO$_2$,5Br-$H_6L^{1,1,4}$ were obtained from reduction of the Schiff base precursors 3Br,5Cl-$H_3L$ and 3NO$_2$,5Br-$H_3L$ (Scheme 1). These Schiff bases are original from this work, although similar to others previously described.[22-23] Both bases were obtained in an analogous manner, exemplified by the isolation of **3Br,5Cl-$H_3L$**: to a methanol (20 mL) solution of 3Br,5Cl-salicylaldehyde (2.028 g, 8.44 mmol), a methanol (20 mL) solution of triethylentetramine (0.420 g, 2.81 mmol) was added. The mixture was stirred in air for 4 h, and a yellow solid precipitated, being subsequently filtered off, washed with diethylether and dried in an oven. Yield: 1.578 g (70%). Elemental analysis calcd. for $C_{27}H_{24}N_4O_3Br_3Cl_3$ (798.58): C 40.61, N 7.02, H 3.03%. Found: C 40.23, N 7.12, H 2.90%. IR (ATR, $\tilde{v}$/cm$^{-1}$): 1633 (C=N$_{imine}$), 3066 (OH). ^{1}H RMN (400 MHz, DMSO-$d_6$, $\delta$ in ppm): 2.66-2.77 (m, 4H, 2H1 + 2H2); 2.81-2.93 (m, 2H, H2); 3.40-3.46 (m, 2H, H1); 3.59-3.72 (m, 4H, H3); 4.09 (s, 1H, H17); 7.21 (s, 1H, H11); 7.39 (s, 2H, H8); 7.44 (s, 1H, H13); 7.67 (s, 2H, H6); 8.38 (s, 2H, H4); 11.85 (s, 1H, OH); 14.38 (s, 2H, 2OH).

**3NO$_2$,5Br-$H_3L$**: 5Br,3NO$_2$-salicyladehyde (0.500 g, 1.97 mmol); triethylentetramine (0.100 g, 0.66 mmol). Yield: 0.43 g (78%). Elemental analysis calcd. for $C_{27}H_{24}N_7O_9Br_3$ (830.24): C 39.06, N 11.81, H 2.91%. Found: C 38.98, N 12.05, H 2.82%. IR (ATR, $\tilde{v}$/cm$^{-1}$): 1646 (C=N$_{imine}$), 3075 (OH). ^{1}H RMN (400 MHz, DMSO-$d_6$, $\delta$ in ppm): 2.72-2.95 (m, 6H, 2H1 + 4H2); 3.40-3.53 (m, 2H, H1); 3.60-4.00 (m, 4H, H3); 4.39 (s, 1H, H17); 7.58 (s, 1H, H11); 7.68 (s, 2H, H6); 7.82 (s, 1H, H13); 8.08 (s, 1H, H8); 8.41 (s, 2H, H$_{imine}$); 13.99 (s, 2H, 2OH).

3Br,5Cl-$H_6L^{1,1,4}$ and 3NO$_2$,5Br-$H_6L^{1,1,4}$ were obtained from the reduction of 3Br,5Cl-$H_3L$ and 3NO$_2$,5Br-$H_3L$, respectively, using a variation of a previously described method.[20-22]

**3Br,5Cl-$H_6L^{1,1,4}$** was obtained as an impure product, mixed with a small quantity of 3Br,5Cl-$H_6L^{1,2,4}$ (*ca.* 10% based on ^{1}H NMR) in agreement with previous results:[20-22] to a suspension of 3Br,5Cl-$H_3L$ (1.578 g, 1.976 mmol) in methanol (25 mL), NaBH$_4$ (0.336 g, 8.892 mmol) was added in small portions for 15 min. The mixture was stirred for 12 h, and the obtained solution was concentrated to dryness in a rotary evaporator. The precipitated white solid was mixed with a NH$_4$CH$_3$COO (1.20 g, 15.584 mmol) water (15 mL) solution. Then, the mixture was extracted with CHCl$_3$ (3 x 15 mL). The extracted organic phases were dried with MgSO$_4$, and then MgSO$_4$ was removed by filtration. The dried solution was concentrated to dryness, and a pale-yellow solid was recovered, and dried in an oven. Yield: 0.620 g (39%). ^{1}H RMN (400 MHz, CDCl$_3$, $\delta$ in ppm): 2.27-3.26 (m, H$_{methylene}$); 3.54-4.11 (m, H$_{methylene}$); 6.73-6.83 (m, H$_{aromatic}$); 7.25-7.40 (m, H$_{aromatic}$)

**3NO$_2$,5Br-$H_6L^{1,1,4}$**: To a suspension of 3NO$_2$,5Br-$H_3L$ (0.420 g, 0.506 mmol) in methanol (25 mL), NaBH$_4$ (0.115 g, 3.036 mmol) was added in small portions for 15 min. The mixture was stirred for 2 h, and the obtained solution was concentrated up to ½ of its initial volume. The precipitated orange solid was filtered and dried in air. Yield: 0.175 g (41%). ^{1}H RMN (400 MHz, DMSO-$d_6$, $\delta$ in ppm): 2.32-2.41 (m, 2H, H3'); 2.80-2.91 (m, 4H); 3.34-3.50 (m, 4H) (2H1 + 2H1' + 2H2 + 2H2'); 3.95 (s, 2H, H4); 4.18 (4H, s, H4'); 7.17 (s, 1H, H6); 7.49 (s, 2H, H11); 7.72 (s, 1H, H8); 7.90 (s, 2H, H13).

## Syntheses of the complexes

All the complexes were obtained in a similar way, exemplified by the isolation of **[Dy(3Br,5Cl-$H_3L^{1,1,4}$)(H$_2$O)]·0.25MeOH (1W·0.25MeOH)**: To a solution of impure 3Br,5Cl-$H_6L^{1,1,4}$ (0.200 g, 0.248 mmol) in chloroform (20 mL), a solution of NaOH (0.030 g, 0.750 mmol) in methanol (10 mL) was added. Then, Dy(NO$_3$)$_3$·6H$_2$O (0.113 g, 0.248 mmol) solved in methanol (10 mL) was also added to the basic ligand solution, and the mixture was stirred for 6 h at room temperature. The obtained solution was left to slowly evaporate, until single crystal of **1W**·0.25MeOH, suitable for X-ray diffraction studies, precipitated. The crystals were filtered and dried in an oven. Yield: 0.102 g (41%). Elemental analysis calcd. for $C_{27.25}H_{30}Br_3Cl_3DyN_4O_{4.25}$ (990.13): C 33.0, N 5.66, H 3.05%. Found: C 32.84, N 5.81, H 2.82%.

Recrystallisation of **1W**·0.25MeOH in pyridine gave single crystals of **1Py**, suitable for X-ray diffraction studies.

**[Dy(3NO$_2$,5Br-$H_3L^{1,1,4}$)(H$_2$O)] (2W)**: 3NO$_2$,5Br-$H_6L^{1,1,4}$ (0.300 g, 0.359 mmol); NaOH (0.043 g, 1.076 mmol), Dy(NO$_3$)$_3$·6H$_2$O (0.164 g, 0.359 mmol). The solution was concentrated up to 1/2 of its volume, and a yellow solid precipitated. The solid was recrystallized in toluene/MeCN, yielding single crystals of [Dy(3NO$_2$,5Br-$H_3L^{1,1,4}$)(H$_2$O)]·2CH$_3$C$_6$H$_5$ (**2W**·2CH$_3$C$_6$H$_5$), suitable for X-ray diffraction studies, which lose the toluene solvate on drying, to give [Dy(3NO$_2$,5Br-$H_3L^{1,1,4}$)(H$_2$O)] (**2W**). Yield: 0.276 g (76%). Elemental analysis calcd. for $C_{27}H_{29}Br_3DyN_7O_{10}$ (1013.78): C 31.99, N 9.67, H 2.88%. Found: C 31.81, N 9.51, H 2.78%.

**[Y(3Br,5Cl-$H_3L^{1,1,4}$)(CH$_3$OH)] (3M)**: 3Br,5Cl-$H_6L^{1,1,4}$ (0.200 g, 0.248 mmol); NaOH (0.030 g, 0.750 mmol); Y(NO$_3$)$_3$·6H$_2$O (0.095 g, 0.248 mmol). The precipitated solid was recrystallised in chloroform/methanol/toluene to yield single crystal of **3M**·CH$_3$C$_6$H$_5$, suitable for X-ray diffraction studies. These crystals lose the toluene solvent on drying, to give **3M**. Yield: 0.095 g (42%). Elemental analysis calcd. for $C_{28}H_{31}Br_3Cl_3N_4O_4Y$ (922.52): C 36.42, N 6.07, H 3.39%. Found: C 36.19, N 6.17, H 3.21%.

**[Y(3NO$_2$,5Br-$H_3L^{1,1,4}$)(H$_2$O)]·H$_2$O (4W·H$_2$O)**: 3NO$_2$,5Br-$H_6L^{1,1,4}$ (0.100 g, 0.120 mmol); NaOH (0.014, 0.36 mmol); Y(NO$_3$)$_3$·6H$_2$O (0.046 g, 0.120 mmol). The obtained solution was concentrated up to 1/3 of its volume, and a yellow solid precipitated. The solid was recrystallized in toluene, yielding a crystalline powder of **4W**·H$_2$O. Yield: 0.037 g (32%). Elemental analysis calcd. for $C_{27}H_{31}Br_3N_7O_{11}Y$ (958.18): C 33.81, N 10.23, H 3.23%. Found: C 33.25, N 10.26, H 2.92%.

Yttrium diluted magnetic samples of [Dy$_{0.1}$Y$_{0.9}$(3Br,5Cl-$H_3L^{1,1,4}$)(CH$_3$OH)$_{0.9}$(H$_2$O)$_{0.1}$] (**1W**@Y), [Dy$_{0.1}$Y$_{0.9}$(3Br,5Cl-$H_3L^{1,1,4}$)(Py)] (**1Py**@Y), and [Dy$_{0.1}$Y$_{0.9}$(3NO$_2$,5Br-$H_3L^{1,1,4}$)(H$_2$O)] (**2W**@Y) were obtained by dissolving 1:10 mixtures of **1W**·0.25MeOH and **3M** in methanol, **1Py** and **3M** in pyridine, and **2W** and **4W**·H$_2$O in methanol, respectively,

stirring overnight at room temperature, and concentrating and collecting the solids under vacuum.

**[Dy$_{0.1}$Y$_{0.9}$(3Br,5Cl-H$_3$L$^{1,1,4}$)(CH$_3$OH)$_{0.9}$(H$_2$O)$_{0.1}$]** **(1W@Y)**: Elemental analysis calcd. for C$_{27.9}$H$_{30.8}$Br$_3$Cl$_3$Dy$_{0.1}$N$_4$O$_4$Y$_{0.9}$ (927.95): C 36.08, N 6.03, H 3.32%. Found: C 35.95, N 5.99, H 3.03%. Micro X-ray fluorescence: Dy:Y ratio 0.09: 0.91.

**[Dy$_{0.1}$Y$_{0.9}$(3Br,5Cl-H$_3$L$^{1,1,4}$)(Py)]** **(1Py@Y)**: Elemental analysis calcd. for C$_{32}$H$_{32}$Br$_3$Cl$_3$Dy$_{0.1}$N$_5$O$_3$Y$_{0.9}$ (976.93): C 39.31, N 7.16, H 3.27%. Found: C 39.38, N 7.17, H 3.23%. Micro X-ray fluorescence: Dy:Y ratio 0.09: 0.91.

**[Dy$_{0.1}$Y$_{0.9}$(3NO$_2$,5Br-H$_3$L$^{1,1,4}$)(H$_2$O)]** **(2W@Y)**: Elemental analysis calcd. for C$_{27}$H$_{29}$Br$_3$Dy$_{0.1}$N$_7$O$_{10}$Y$_{0.9}$ (947.51): C 34.19, N 10.34, H 3.06%. Found: C 34.28, N 10.51, H 3.18%. Micro X-ray fluorescence: Dy:Y ratio 0.09: 0.91.

### Crystallographic refinement and structure solution

Crystal data and details of refinement are given in Table S1. The single crystals of **1W**·0.25MeOH, **1Py**, **2W**·2CH$_3$C$_6$H$_5$ and **3M**·CH$_3$C$_6$H$_5$ could be obtained as detailed above. Data were collected at 100 K on a Bruker D8 VENTURE PHOTON III-14 diffractometer, employing graphite monochromatised Mo-kα (λ = 0.71073 Å) radiation. Multiscan absorption corrections were applied using either the SADABS or the TWINABS routine,[24] in this latter case for **1W**·0.25MeOH. The structures were solved by standard direct methods employing SHELXT,[25] and then refined by full matrix least-squares techniques on $F^2$ by use of SHELXL, from the program package SHELX-2018.[25] All atoms different of hydrogen were anisotropically refined, with some exceptions related to disordered solvates with low occupation sites, which in some cases also needed some restraints. H atoms were typically included in the structure factor calculations in geometrically idealized positions. However, with the intention of revealing the hydrogen bonding scheme, hydrogen atoms attached to amine nitrogen atoms or to water molecules were located in the corresponding Fourier maps. In this case, either they were freely refined, or with thermal parameters derived from their parent atoms.

### Powder X-ray diffraction studies

The powder diffractogram for **1Py** was recorded on a Philips diffractometer with a control unity type "PW1710", a vertical goniometer type "PW1820/00" and a generator type "Enraf Nonius FR590", operating at 40 kV and 30 mA, using monochromated Cu-Kα (λ = 1.5418 Å) radiation. A scan was performed in the range 2 < 2θ < 30° with t = 3 s and Δ2θ = 0.02°. LeBail refinement was obtained with the aid of HighScore Plus Version 3.0d.

### Magnetic measurements

Magnetic susceptibility dc measurements for microcrystalline samples of **1W**·0.25MeOH, **1Py**, and **2W**, and ac measurements for **1W**·0.25MeOH, **1Py**, **2W**, **1W@**Y, **1Py@**Y, and **2W@**Y were carried out with a PPMS Quantum Design susceptometer. The dc magnetic susceptibility data were recorded under a magnetic field of 1000 Oe in the range 2-300 K. Magnetisation measurements at 2.0 K were recorded under magnetic fields ranging from 0 to 70000 Oe. Diamagnetic corrections were estimated from Pascal's Tables. Alternating current (ac) susceptibility measurements for all the undiluted samples were recorded under zero and 1000 Oe dc fields, with an oscillating ac field of 10 Oe, and ac frequencies ranging from

50 to 10000 Hz. The ac measurements for **1W@**Y, **1Py@**Y, and **2W@**Y were recorded at $H_{dc}$ = 0 Oe.

### Computational Details

OpenMolcas[26] was used to perform CASSCF-SO calculations on all complexes to determine their electronic structure. The molecular geometries from the single crystal XRD structure with no optimization were used, taking the largest disorder component only. Basis sets from ANO-RCC library[27-28] were employed with VTZP quality for Dy atoms, VDZP quality for coordinating atoms (4 nitrogen and 4 oxygen atoms), and VDZ quality for all remaining atoms, employing the second-order DKH transformation. Cholesky decomposition of the two-electron integrals with a threshold of $10^{-8}$ was performed to save disk space and reduce computational demand. The molecular orbitals (MOs) were optimized in state-averaged CASSCF calculations within each spin manifold, considering 21, 224 and 490 roots for spin sextet, quartet and doublet, respectively – for each spin multiplicity, the number of states mixed by spin orbit coupling are 21, 128 and 130, respectively. The resulting spin-orbit wavefunctions were decomposed into their crystal field (CF) wavefunctions, and the magnetic susceptibility was calculated using SINGLE_ANISO.[29] The electronic structure of the non-Gd lanthanide ions is well described by the standard CF Hamiltonian:

$$\widehat{H}_{CF} = \sum_{k=2,4,6} \sum_{q=-k}^{k} B_k^q \, \theta_k \widehat{O}_k^q$$

where $B_k^q$ are the CF parameters, $\theta_k$ are the operator equivalent factors and $\widehat{O}_k^q$ are the extended Steven's operator equivalents.[30] To address the effect of structural disorder on the electronic structure of the compounds, we also performed gas-phase geometry optimisations with density functional theory (DFT, see SI for details).

## Results and discussion

The condensation of 3Br,5Cl-salicylaldehyde or 3NO$_2$,5Br-salicylaldehyde with triethylenetetramine in 1:3 molar ratio, according to a procedure previously described,[22,23] yields the new Schiff bases 3Br,5Cl-H$_3$L and 3NO$_2$,5Br-H$_3$L (Scheme 1), respectively, which were satisfactorily characterised by elemental analysis, IR and $^1$H NMR spectroscopies. Reduction of these bases with NaBH$_4$ leads to different results (Scheme 1). Thus, the reduction of 3Br,5Cl-H$_3$L yields a mixture of both 3Br,5Cl-H$_6$L$^{1,2,4}$ and 3Br,5Cl-H$_6$L$^{1,1,4}$ isomers, as it occurs with the non-substituted ligand H$_3$L,[20-22] but in this case the equilibrium is shifted towards the 3Br,5Cl-H$_6$L$^{1,1,4}$ species (*ca.* 90% based on $^1$H NMR). By contrast, the reaction of 3NO$_2$,5Br-H$_3$L with sodium borohydride only produces pure 3NO$_2$,5Br-H$_6$L$^{1,1,4}$ (Scheme 1).

The mixture of 3Br,5Cl-H$_6$L$^{1,2,4}$ and 3Br,5Cl-H$_6$L$^{1,1,4}$, as well as pure 3NO$_2$,5Br-H$_6$L$^{1,1,4}$, react with dysprosium nitrate to yield the corresponding [Dy(3R$_1$,5R$_2$-H$_3$L$^{1,1,4}$)(H$_2$O)]·nsolvate complex (Scheme 1), indicating that the small proportion of 3Br,5Cl-H$_3$L$^{1,2,4}$ does not longer exist once it is coordinated to the metal ion. This result seems to disagree with those found with H$_6$L$^{1,1,4}$ and H$_6$L$^{1,2,4}$ mixtures.[20-22] In this latter case, where the aromatic rings do not have substituents, the pH of the medium seems to play a fundamental role in the equilibrium, and when the mixture of isomers is mixed with NaOH in 1:3 molar ratio, as in this study, the equilibrium seems to
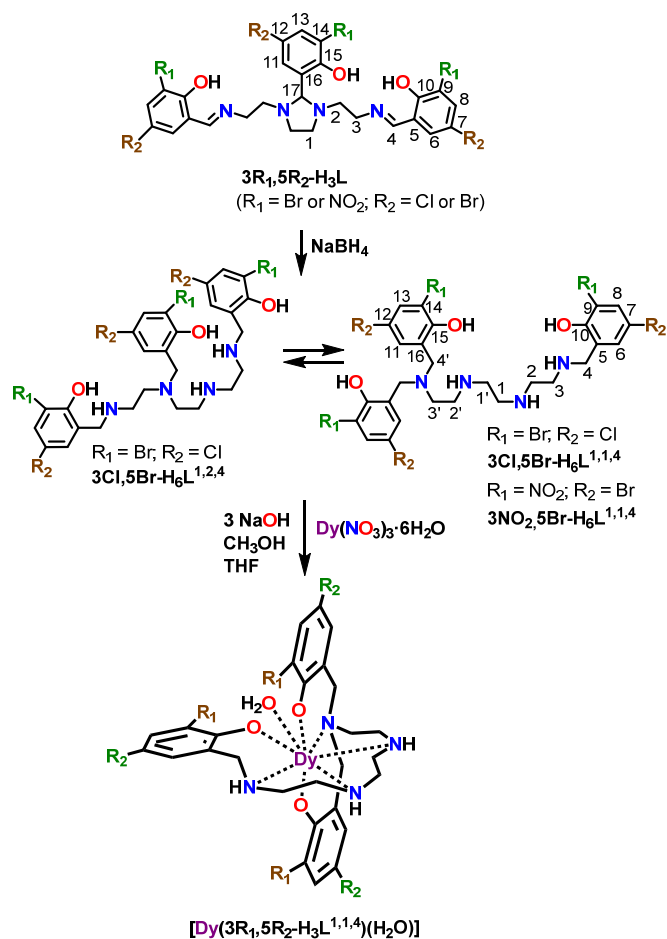
**Scheme 1** Reaction scheme for the isolation of the complexes, with numbering schemes for ^{1}H NMR studies.

shift towards the $H_6L^{1,2,4}$ species.[20-22] In our case study, this equilibrium is clearly shifted towards the $3R_1,5R_2$-$H_6L^{1,1,4}$ isomer, and this could be maybe related to the presence of electron-withdrawing substituents on the aromatic ring, and/or to the presence of substituents that cause steric hindrance.

[Dy(3Br,5Cl-$H_3L^{1,1,4}$)($H_2O$)]·0.25MeOH (**1W**·0.25MeOH) was obtained in the form of single crystals from the reaction mixture, while the isolated solid from the reaction of $3NO_2,5Cl$-$H_6L^{1,1,4}$ and dysprosium nitrate precipitates as a yellow powder, whose recrystallisation in toluene/MeCN yields single crystals of [Dy(3NO$_2$,5Br-$H_3L^{1,1,4}$)($H_2O$)]·2CH$_3$C$_6$H$_5$ (**2W**·2CH$_3$C$_6$H$_5$). These crystals lose the toluene solvate on drying, to generate [Dy(3NO$_2$,5Br-$H_3L^{1,1,4}$)($H_2O$)] (**2W**). Likewise, recrystallisation of **1W**·0.25MeOH in pyridine affords [Dy(3Br,5Cl-$H_3L^{1,1,4}$)(Py)] (**1Py**) as single crystals. The comparison of the experimental powder X-ray diffractogram of the crystalline product **1Py** with the calculated one from single X-ray diffraction data (Fig. S1) demonstrates that **1Py** has been obtained with high purity, without mixtures, and that the collected sample and the solved single crystal are the same compound.

In addition, diamagnetic yttrium complexes [Y(3Br,5Cl-$H_3L^{1,1,4}$)(MeOH)] (**3M**) and [Y(3NO$_2$,5Br-$H_3L^{1,1,4}$)($H_2O$)]·$H_2O$ (**4W**·$H_2O$), analogous to the dysprosium compounds **1W** and **2W**, could be isolated in comparable syntheses. Recrystallisation of **3M** in

toluene also yields single crystals of **3M**·CH$_3$C$_6$H$_5$, which loses the solvate on drying.

### X-ray diffraction studies

The crystal structures of the three dysprosium compounds [Dy(3Br,5Cl-$H_3L^{1,1,4}$)($H_2O$)]·0.25MeOH (**1W**·0.25MeOH), [Dy(3Br,5Cl-$H_3L^{1,1,4}$)(Py)] (**1Py**) and [Dy(3NO$_2$,5Cl-$H_3L^{1,1,4}$)($H_2O$)]·2CH$_3$C$_6$H$_5$·(**2W**·2CH$_3$C$_6$H$_5$) are very similar, and they will be discussed together. The unit cells of all of them contain [Dy(3R$_1$,5R$_2$-$H_3L^{1,1,4}$)(D)] (R$_1$ = Br or NO$_2$, R$_2$ = Cl or Br, D = $H_2O$ or Py) neutral molecules and, in the case of **1W**·0.25MeOH and **2W**·2CH$_3$C$_6$H$_5$, different solvates. The main differences among these complexes lie in the substituents on the phenol rings of the ligand (3Br,5Cl for **1W** and **1Py** and 3NO$_2$,5Br for **2W**), in the ancillary D ligand (water in **1W** and **2W**·CH$_3$C$_6$H$_5$, and pyridine in **1Py**), and in the number of chemically equivalent but crystallographically different complex molecules in their asymmetric units: one for **1Py** and two for **1W**·0.25MeOH (namely **1W**.1 and **1W**.2) and **2W**·2CH$_3$C$_6$H$_5$ (namely **2W**.1 and 2W.2). It is remarkable that the water ligand in **1W**.2, and the nitro substituent of one of the terminal arms of the aminophenol donor in **2W**.2, are disordered over two sites. Ellipsoids diagrams for **1W**.1, **1Py** and **2W**.2 are shown in Fig. 1, S2 and S3, respectively, and main distances and angles are recorded in Table S2.

In all these complexes, the aminophenol ligands act as trianionic heptadentate donors, using all their nitrogen and oxygen atoms to bind the metal ion, and the coordination sphere around the dysprosium centre is completed by a pyridine (**1Py**) or a water (**1W** and **2W**·2CH$_3$C$_6$H$_5$) molecule coming from the solvent of the media. The three protonated secondary amine N atoms of the coordinated ligand (NX2, NX3, NX4, with X = 1 or 2) are asymmetric centres, and therefore the [Dy(3R$_1$,5R$_2$-$H_3L^{1,1,4}$)(D)] complexes are chiral. It could be worthy to mention that the two different crystallographic molecules present in the unit cell of **1W** (**1W**.1 and **1W**.2) are
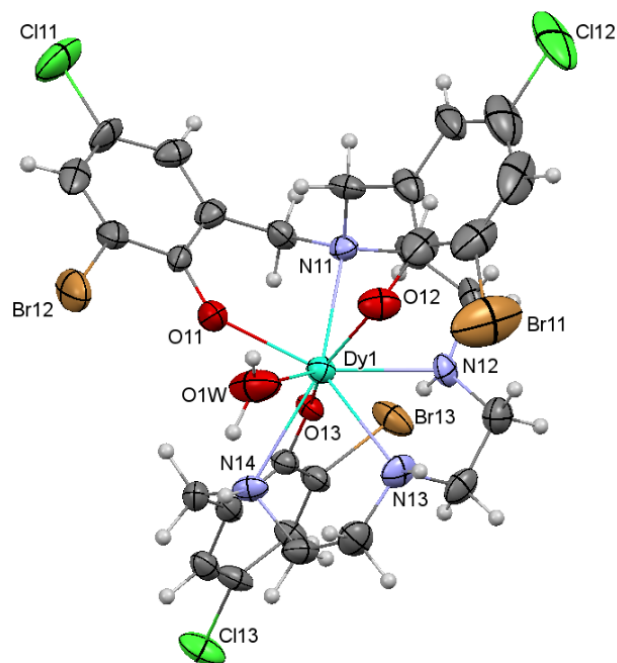


**Fig. 1** Ellipsoid (50% probability) diagram for the (*S,R,R*) enantiomorph of **1W**.1.

enantiomorphs, with (S,R,R) and (R,S,S) configurations, and, therefore, the crystals are racemic.

In the case of **2W**·2CH₃C₆H₅, although their crystals are globally racemic, they are forming a conglomerate of both enantiomeric crystals after spontaneous resolution. Curiously, in each crystal, both **2W**.1 and **2W**.2 molecules are the same enantiomer. Thus, in the case of the solved crystal, both complex units show (R,S,S) configuration. Regarding to polar crystals of **1Py**, we can indicate that although polar crystals are racemic, they show a polar direction were only each enantiomer is present.[31-32]

All the described features lead to $DyN_4O_4$ (**1W** and **2W**) or $DyN_5O_3$ (**1Py**) environments for the complexes. Calculations of the distortion from an ideal eight-vertex polyhedron with the SHAPE program[33] indicate that the geometry for these compounds is between square antiprism, biaugmented trigonal prism and triangular dodecahedron (Table S3). The main distances and angles about the metal centres (Table S2) agree with those expected for dysprosium complexes with N,O donors.[19,21] In spite of this, a difference in the Dy-O$_{phenoxide}$ bond distances is remarkable: in **1Py**, the Dy1-O12 and Dy1-O13 bonds, which form a O-Dy-O angle of ca. 148.7°, are the shortest ones, while for **1W** and **2W** there is not such a defined axis. In addition, the Dy1-O12 and Dy1-O13 bond distances in **1Py** are noticeably shorter than the corresponding DyX-OX2 and DyX-OX3 distances in **1W** and **2W** (Table S2). Besides, in general, all the other Dy-N$_{aminophenol}$ and Dy-O$_{aminophenol}$ bonds for **1Py** are shorter than the homologous ones in **1W** and **2W**, and these bonds are in most cases shorter for **1W** than for **2W**. On the contrary, Dy-OXw bonds in **1W** are longer than in **2W**. Accordingly, these data agree with the greater donor character of the aminophenol with the less electron-withdrawing substituents on the phenol ring (3Br,5Cl-H₆L$^{1,1,4}$), and with the fact that the presence of a nitrogen auxiliary donor makes the aminophenol donate more charge with respect to an oxygen donor, shortening the Dy-X$_{aminophenol}$ bonds.

The asymmetric unit of [Y(3Br,5Cl-H₃L$^{1,1,4}$)(CH₃OH)]·CH₃C₆H₅ (**3M**·CH₃C₆H₅) contains two chemically equivalent but crystallographically different [Y(3Br,5ClH₃L$^{1,1,4}$)(CH₃OH)] neutral molecules, which will be called **3M**.1 and **3M**.2, and toluene as solvate. An ellipsoid diagram for **3M**.1 is shown in Fig. S4, and main distances and angles in Table S4. The structure of **3M** is completely comparable with that of **1W**, and the main difference, in addition to the nature of the central metal ion, is that the water ancillary donor in **1W** has been replaced by a methanol donor in **3M**. Accordingly, the aminophenol ligand is also acting as heptadentate in **3M**, where the methanol ligand completes the $YN_4O_4$ coordination spheres of the yttrium atoms in both **3M**.1 and **3M**.2. Calculations with the SHAPE program also indicate that the geometry about the Y³⁺ ion in **3M**.2 is between square antiprism and biaugmented trigonal prism, but in **3M**.1 the geometry is closer to a triangular dodecahedron (Table S3). In these polyhedrons, all the distances and angles are in the range of those expected,[22,34] and do not merit further consideration.

Finally, it is worth of mention that **3M** is also a case of spontaneous resolution, as both **3M**.1 and **3M**.2 complexes of the solved unit cell are the same (S,R,R) enantiomer, and the crystals belong to a Sohnke space group. This contrasts with the racemic character found for the asymmetric unit of **1W**·0.25MeOH.

## Magnetic Properties

Direct-current (dc) magnetic susceptibility measurements were recorded for **1W**·0.25MeOH, **1Py** and **2W** as a function of the temperature. The plots of $\chi_M T$ vs $T$ are shown in Fig. 2 and S5. The $\chi_M T$ values for the complexes at 300 K are in the range 13.5-14.6 cm³Kmol⁻¹, which are very close to the expected ones for one uncoupled Dy³⁺ ion at room temperature (14.17 cm³Kmol⁻¹). The experimental curves continuously decrease until 2 K, reaching $\chi_M T$ values of 9.9, 11.5 and 7.3 cm³Kmol⁻¹ for **1W**·0.25MeOH, **1Py** and **2W**, respectively. This drop in the curves can be mainly ascribed to thermal depopulation of the excited Kramers doublets, which arise from the split of the ground $^6H_{15/2}$ term by crystal field effects.

The field dependence of the reduced magnetisation at 2 K at the maximum applied field of 70000 Oe tends to 4.1, 4.7 and 4.9 Nμ$_B$ for **1W**·0.25MeOH, **1Py** and **2W**, respectively (Fig. 2 and S5, inset), values that are far away from the theoretical saturation one initially anticipated for an isolated Dy$^{III}$ ion (10 Nμ$_B$), but very close to the value of 5 Nμ$_B$ for a highly anisotropic Dy$^{III}$ ion with an Ising-like ground doublet.[35]

The dynamic magnetic properties of the three mononuclear complexes were also studied, and **1W**·0.25MeOH and **1Py** show out-of-phase peaks of the susceptibility ($\chi''_M$) as a function of the frequency above 2 K (Fig. 3). However, **2W** shows frequency and temperature dependence of $\chi''_M$, but without peaks (Fig. S6). Thus, these results seem to indicate that **1W**·0.25MeOH and **1Py** are SIMs, while for **2W** either the energy barrier is too small to observe peaks in the $\chi''_M$ vs frequency plot, or the quantum tunnelling of the magnetisation prevents the observation of any other magnetic relaxation process.

The shape of the Arrhenius plots (Fig. S7) and the α parameters extracted from the Cole-Cole plots using a generalised Debye model (Fig. S8, Table S5) for **1W**·0.25MeOH and **1Py** indicate a large distribution of relaxation times. The Arrhenius plots (Fig. S7,) show that the data deviate from linearity in the low-temperature region, but that it is linear above 3.3 K for **1W**·0.25MeOH, and above 10 K for **1Py**. This linearity could indicate an Orbach relaxation process. Thus, assuming that only the Orbach relaxation predominates at high temperatures, fitting this region with equation 1 affords $U_{eff}$ = 0.8 K,
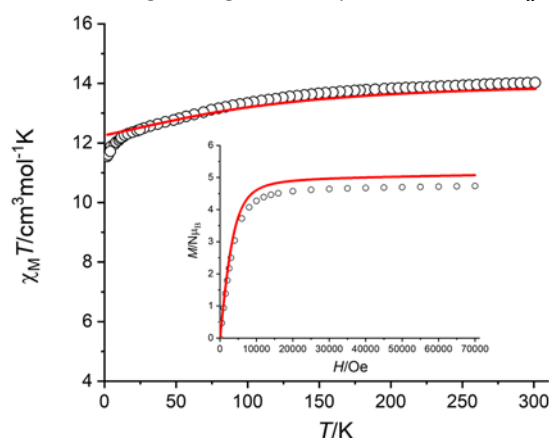


**Fig. 2** $\chi_M T$ vs $T$ for **1Py**. Inset: $M$/Nμ$_B$ vs $H$ at 2 K. The solid red lines represent the theoretical data obtained from ab initio calculations (with CASSF-SO methodology).
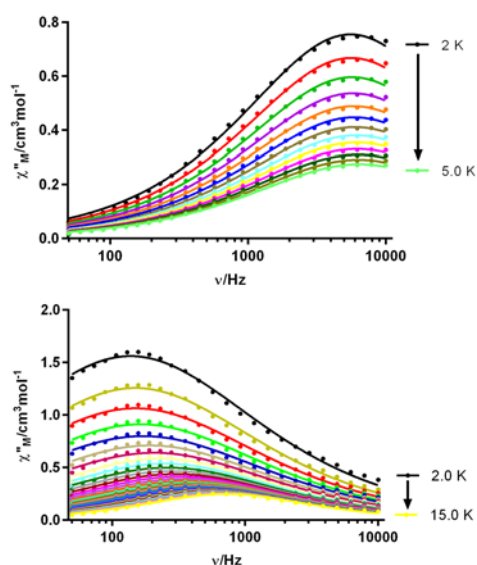
**ARTICLE**                                                                                               Dalton Trans.



**Fig. 3** Frequency dependence of $\chi''_M$ at different temperatures in a zero applied field for: up) **1W·0.25MeOH**; bottom) **1Py**.

with $\tau_0$ = 5.7x10$^{-8}$ s for **1W·0.25MeOH**, and $U_{eff}$ = 17.4 K, with $\tau_0$ = 5.9x10$^{-8}$ s for **1Py**.

$$\tau^{-1} = \tau_0^{-1}e^{-U_{eff}/k_BT} \quad (1)$$

The energy difference between the ground and first excited state calculated by *ab initio* studies (*vide infra*) strongly disagrees with the effective barrier determined from ac measurements using the Orbach model in the linear region (*ca* 300 K *vs* less than 18 K, respectively). This discards an Orbach process and suggests a combination of other different relaxation mechanisms, including QTM relaxation, as it can be inferred from $\chi''_M$ *vs T* graphs (Fig. S9).

Thus, taking into account that the aim of this work is to see the influence of the phenol substituents and the ancillary donors on the relaxation energy barrier, attempts were made to eliminate the quantum channel in order to appreciate the energy gap for the spin reversal. Accordingly, we investigated the dynamical response of the samples under a small static magnetic field. Under an optimised field of 1000 Oe (Fig. S10), the three complexes show frequency dependence of the out of-phase susceptibility (Fig. 4), with maxima for $\chi''_M$ in all cases.

Once again, the Arrhenius plots (Fig. 5) show that the data deviate from linearity in all cases, and Cole-Cole plots (Fig. S11) show α values ranging from 0.09 to 0.6 (Table S5), suggesting the possible existence of more than one relaxation process. Consequently, the Arrhenius plots were fitted employing Orbach, Direct, Raman, and QTM processes (equation 3).

$$\tau^{-1} = \tau_0^{-1}e^{-U_{eff}/k_BT} + AT + CT^n + \tau_{QTM}^{-1} \quad (2)$$

For the three complexes, the best fit considering all these processes, individually or grouped, is achieved with Orbach and Raman processes (Table 1), and attempts of fits including QTM relaxation were unsuccessful, despite the tails of $\chi''_M$ at low temperatures (Fig. S12). This may be because $\chi''_M$ peaks only appears above 8.0 K for **1W·0.25MeOH**, 12 K for **1Py** and 4 K for **2W**, and probably this effect is not important in these complexes at so high temperatures.
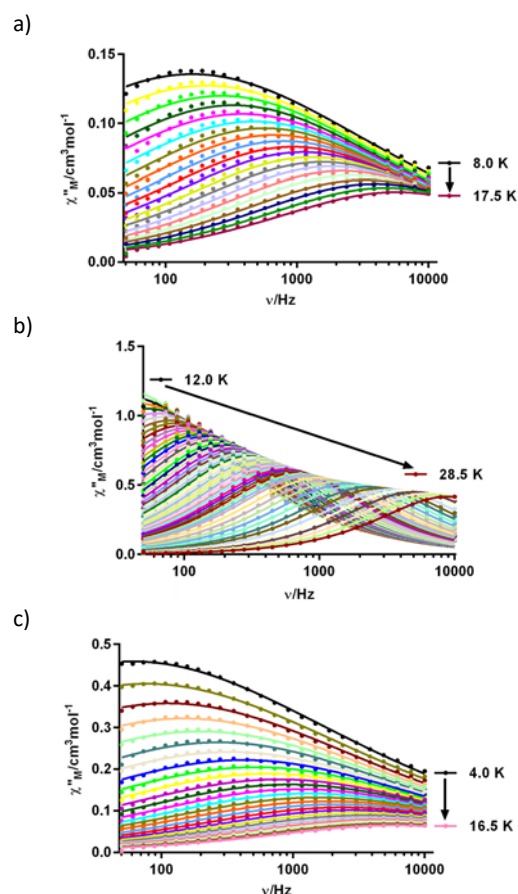


**Fig. 4** Frequency dependence of $\chi''_M$ at different temperatures in an applied field of 1000 Oe for: a) **1W·0.25MeOH**; b) **1Py**; c) **2W**.

In an attempt to gain more insight into the QTM origin, the influence of intermolecular dipole-dipole interactions was studied by the magnetic site dilution. Accordingly, diluted samples **1W@Y**, **1Py@Y** and **2W@Y** were prepared and new ac measurements in zero dc field recorded (Fig. S13 and S14), showing peaks for $\chi''_M$ *vs* ν in all cases. The best fits of the higher temperature regions of the Arrhenius' plots (Fig. S15) according to equation 1 renders once more very low $U_{eff}$ values, below 31 K for all the complexes, in disagreement with the calculated zero-field *ab initio* values. Thus, once again, this discards an Orbach relaxation. In addition, the shape of the $\chi''_M$ *vs T* graphs clearly show that the quantum channel is still present. Consequently, these results seem to indicate that the elimination of the dipolar intermolecular interactions does not quench the QTM process, suggesting the importance of the hyperfine interactions. In addition, it is worth mentioning that, as usual, the effect of the magnetic field in quenching QTM is more important than that provoked by magnetic dilution.

**Table 1**. Fit parameters of the temperature dependence of the relaxation time for **1W·0.25MeOH**, **1Py** and **2W** in $H_{dc}$.= 1000 Oe

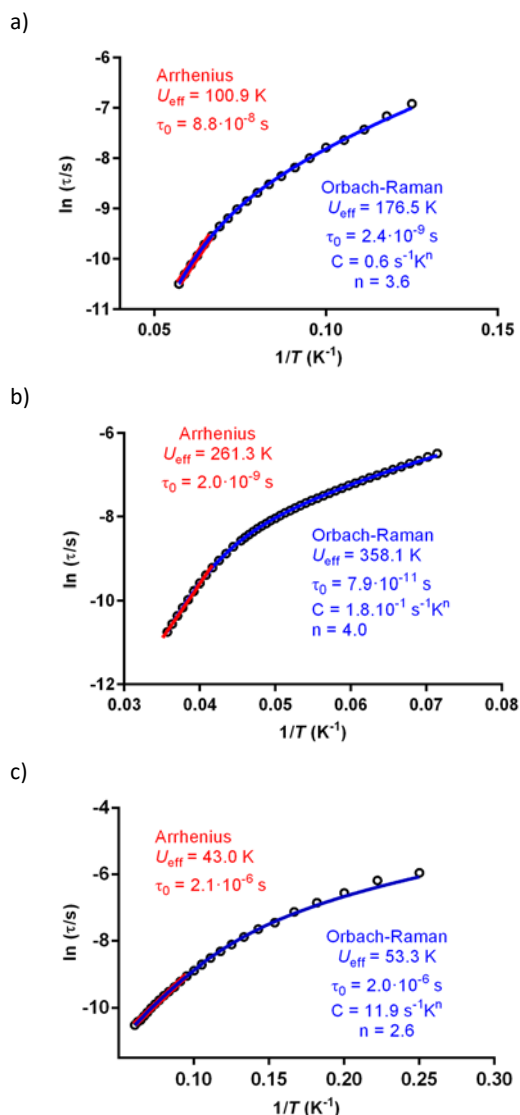| | *Orbach* | | *Raman* |
|---|---|---|---|
| *Complex* | $U_{eff}$ (K) | $\tau_0$ (10$^{-9}$ s) | n / C (s$^{-1}$K$^{-n}$) |
| **1W·0.25MeOH** | 176.5 | 2.4 | 3.6 / 0.6 |
| **1Py** | 358.1 | 0.079 | 4.0 / 1.8·10$^{-1}$ |
| **2W** | 53.3 | 2000 | 2.6 / 11.9 |

a)



b)



c)



**Fig. 5** Arrhenius plot in $H_{dc}$ = 1000 for: a) **1W**·0.25MeOH; b) **1Py**; c) **2W**. The solid lines account for the best fit considering only Orbach relaxation (red) or combined relaxation processes (blue, see text).

As a summary of the ac studies, it must be pointed out that the effective energy barriers, calculated in the presence of a magnetic field, follow the sequence: **1Py > 1W**·0.25MeOH > **2W**. Given that the main difference between **1Py** and **1W**·0.25MeOH is the ancillary water ligand ($H_2O$ in **1W** and Py in **1Py**), this study demonstrates that the introduction of a nitrogen instead of an oxygen donor favours the anisotropy in distorted square antiprism $Dy^{III}$ complexes. This seems to be related with the $Dy$-$O_{phenoxide}$ distances, as previously discussed. Thus, in the case of **1Py**, the shortest $Dy$-$O$ bond distances are $Dy1$-$O12$ and $Dy1$-$O13$, with an $O12$-$Dy1$-$O13$ angle of 148.65(11). These distances are significantly shorter than the remaining $Dy$-$O$ or $Dy$-$N$ bonds. This distribution of the shortest $Dy$-$O_{phenoxide}$ bonds in the $Dy^{3+}$ coordination sphere favours an axial ground state with its anisotropy axis lying close to the $O12$-$Dy$-$O13$ direction. However, in the case of **1W**·0.25MeOH, the $Dy$-$O_{phenoxide}$ distances (Table S2) are longer than in **1Py**, and there is not so clear two shortest $Dy$-$O$ bonds. The same occurs for **2W**, and in this case, the worse magnetic behaviour of **2W** respect to **1W**·0.25MeOH could be ascribed to the

more electron-withdrawing character of the nitro and bromine substituents on the aromatic rings in comparison with the chlorine and bromine ones. A prominent reduction of $U_{eff}$ by means of electron-withdrawing non coordinating groups was previously reported for pseudo-pentagonal bipypramidal complexes,[36] but the influence of these aromatic ring substituents on the magnetic properties is still poorly studied, and it seems to cause opposite effects in mononuclear[36] and dinuclear systems.[37,38]

**Electronic Structure calculations**

CASS-SO calculations (see Computational details section) were performed to determine the electronic structure of the synthesised compounds. We have considered six molecular structures: **1W**.1 (without solvent), **1W**·2 (without solvent), **1Py**, **2W**.1 (without solvent), **2W**.1toluene (with solvent), and **2W**.2 (without solvent),a and the results are shown in Tables S6, S8 and S10. The **1W**·2 and **2W**.2 moieties show disorder in the water molecule, and in one of the nitro groups, respectively, and only the largest disorder component was taken into account.

We find a reasonable agreement with the experimental susceptibility and magnetisation curves (see Fig. 2 and S5), particularly for **1Py**. The uncertainty generated by the H positions of the water molecule directly coordinated to the Dy ion in **1W** and **2W** might be the responsible for the larger differences observed for these latter compounds compared to **1Py**.[39] This is not improved at the gas-phase optimised structures, which present a noticeable different electronic structure (Table S7, S9 and S11), despite being similar to the crystal structures (Table S12 and Fig. S16). We also note that the results do not depend on the initial starting geometry (**1W**.1 or **1W**.2, **2W**.1 or **2W**.2), as the converged structures are identical. Thus, we hypothesise that the structurally flexible nature of the $[3R_1,5R_2$-$H_3L^{1,1,4}]^{3-}$ ligand is responsible for the very large alpha values from the generalised Debye model.[40]

The CASSCF-SO energy values for the two low-lying Kramers doublets (KDs), as well the respective $g$ tensor values for the six systems, are presented in Table 2. The calculated $g$-factors indicate an easy-axis character for all compounds (Table 2, S6, S8, S10).

As discussed in the crystallographic section, **1W** and **2W**, present two unique molecules within the unit cell. For **1W**, the electronic structure of both complexes is quite similar, with a difference

**Table 2**. Calculated $g$-factors of the ground and first excited states and the angle between their $g_z$ vectors for the six studied systems obtained from CASSCF-SO at the crystal structure.

| Compound | E (cm$^{-1}$) | $g_x$ | $g_y$ | $g_z$ | $\gamma$ (°) |
|---|---|---|---|---|---|
| **1W**.1 | 0.0 | 0 | 0 | 19.80 | -- |
| | 202.42 | 0.71 | 1.62 | 16.83 | 47.1 |
| **1W**.2 | 0.0 | 0.01 | 0.02 | 19.81 | -- |
| | 186.84 | 0.89 | 1.84 | 17.54 | 59.3 |
| **1Py** | 0.0 | 0.01 | 0.01 | 19.80 | -- |
| | 226.04 | 0.29 | 0.41 | 16.98 | 15.7 |
| **2W**.1 | 0.0 | 0.02 | 0.03 | 19.68 | -- |
| | 82.42 | 0.20 | 0.24 | 19.52 | 79.6 |
| **2W**.2 | 0.0 | 0.00 | 0.00 | 19.74 | -- |
| | 168.74 | 0.77 | 1.51 | 18.30 | 73.8 |
| **2W**.1toluene | 0.0 | 0.02 | 0.03 | 19.68 | -- |
| | 72.43 | 0.17 | 0.21 | 19.55 | 79.8 |

between their respective energy gaps (energy difference between the ground and first excited KDs) of *ca.* 15 cm^{-1} (Tables 2 and S6). For **2W**, the much larger difference (Tables 2 and S10) could be ascribed to the disordered nitro group in **2W**.2, and the relative angle of the axial water with respect to the central metal ion.[39] Besides, the calculations for **2W**.1 with and without the toluene solvent yield quite similar parameters, indicating that the trapped solvates do not seem to play an important role in the electronic structure and magnetic properties of these compounds.

Thus, the comparison of the calculated barriers and those obtained by *ab initio* studies shows that the energy barriers follow the same sequence: **1Py** > **1W** > **2W**, and that the theoretical calculated (226 cm^{-1}) and experimentally obtained (248.9 cm^{-1}) barrier for **1Py** are very similar. However, for **1W** and **2W** the experimental and theorical data differ more than for **1Py**. In these two cases, there is a water molecule coordinated to the metal ion, and the uncertainty of the positions of the hydrogen atoms can contribute to this fact,[19c,39] as well as the uncertainty in the position of the nitro groups (**2W**.2). Besides, it should be noted that the crystallographic data indicate that the water molecules establish intermolecular interactions, which are not considered in the calculations. Despite this, the *ab initio* data clearly support the experimental results, given that the tendency in the energy of the barriers is the same.

## Conclusions

Three new mononuclear Dy[III] complexes of two unreported heptadentate aminophenol ligands were fully characterised, showing that the presence of the electron-withdrawing or steric hindrance substituents on the phenol rings favour the isolation of compounds containing the $[3R_1,5R_2-H_3L^{1,1,4}]^{3-}$ isomer. Thus, these complexes contribute to understand the coordination chemistry of Ln with this scarcely reported kind of ligand. The magnetic properties of the three mononuclear distorted octacoordinated Dy[III] complexes have been studied, both experimentally and theoretically. These studies show that **1**·0.25MeOH and **1Py** are SIMs, while **2W** only shows SIM-like behaviour in the presence of a dc field. This external field removes at least partially the quantum channel of the magnetisation, which allows to observe energy barriers as high as 358 K for **1Py**. The magnetic analysis of diluted **1W@Y**, **1Py@Y** and **2W@Y** indicates that the elimination of dipolar interactions does not favour Orbach relaxation. Comparison of the $U_{eff}$ values for the three complexes (**1Py > 1W**·0.25MeOH > **2W**) shows that the energy gap diminishes when the electron-withdrawing character of the substituents on the phenol rings increases, as well as when the ancillary pyridine nitrogen donor is replaced by a water oxygen donor in the distorted square antiprism environment of the dysprosium atom. All these results are supported by *ab initio* calculations. Accordingly, this study delves into the factors that influence the energy barriers in lanthanoid SIMs, and, therefore, it represents a new contribution to the parameters to be considered when designing high performance SIMs.

## Conflicts of interest

There are no conflicts to declare.

## References

1.  J. D. Rinehart and J. R. Long, *Chem. Sci.*, 2011, **2**, 2078–2085.
2.   S. T. Liddle and J. van Slageren, *Chem. Soc. Rev.,* 2015, **44**, 6655—6669
3.  S. Gomez-Coca, D. Aravena, R. Morales and E. Ruiz, *Coord. Chem. Rev.*, 2015, **289**, 379-392.
4.  S. K. Gupta and R. Murugavel, *Chem. Commun.*, 2018, **54**, 3685-3696.
5.  Z. Zhu, M. Guo, X-L. Li and J. Tang, *Coord. Chem. Rev.*, 2019, **378**, 350–364.
6.  A. Zabala-Lekuona, J. M. Seco and E. Colacio, *Cood. Chem. Rev.*, 2021**, 441**, 213984-214020.
7.  (a) F-S. Guo, B. M. Day, Y-C. Chen, M-L. Tong, A. Mansikkam-ki and R. A. Layfield, *Angew. Chem. Int. Ed*., 2017, **56**, 11445–11449. (b) C. A. P. Goodwin, F. Ortu, D. Reta, N. F. Chilton and D. P. Mills, *Nature*, 2017, **548**, 439–442.
8.  K. R. McClain, C. A. Gould, K. Chakarawet, J. S. Teat, T. J. Groshens, J. R. Long and B. G. Harvey, *Chem. Sci*., 2018, **9**, 8492-8503.
9.  F-S. Guo, B. M. Day, Y-C. Chen, M-L. Tong, A. Mansikkam-ki and R. A. Layfield, *Science*, 2018, **362**, 1400-1403.
10. Y-C. Chen, Liu, L. Ungur, J. Liu, Q-W. Li, L-F. Wang, Z-P. Ni, L. F. Chibotaru, X-M. Chen and M-L. Tong, *J. Am. Chem. Soc*., 2016, **138**, 2829-2837.
11. Y.-S. Ding, N. F. Chilton, R. E. P. Winpenny and Y.-Z. Zheng, *Angew. Chem., Int. Ed*., 2016, **55**, 16071-16074.
12. J. Liu, Y-C. Chen, J-L. Liu, V. Vieru, L. Ungur, J-H. Jia, L. F. Chibotaru, Y. Lan, W. Wernsdorfer, S. Gao, X-M. Chen and M-L. Tong, *J. Am. Chem. Soc*., 2016, **138**, 5441–5450.
13. A. B. Canaj, M. K. Singh, C. Wilson, G. Rajaraman and M. Murrie, *Chem. Commun*., 2018, **54**, 8273-8276.
14. Y.-S. Ding, T. Han, Y-Q. Zhai, D. Reta, N. F. Chilton, R. E. P. Winpenny and Y-Z. Zheng, *Chem. Eur. J*., 2020, **26**, 5893–5902.
15. K-X. Yu, J. G. C. Kragskow, Y-S. Ding, Y-Q. Zhai, D. Reta, N. F. Chilton and Y-Z. Zheng, *Chem* 2020, **6**, 1777–1793.
16. L. Zhu, B. Yin, P. Ma and D. Li, *Inorg. Chem*., 2020, **59**, 16117-16121.
17.  P. Kalita, J. Acharya and V. Chandrasekhar, *J. Magn. Magn. Mater.*, 2020**, 498**, 166098.
18. S. Bala, G-Z. Huang, Z-Y. Ruan, S-G. Wu, Y. Liu, L-F. Wang, J-L. Liu and M-L. Tong, *Chem. Commun.,* 2019, **55**, 9939—9942.
19. (a) M. Fondo, J. Corredoira-Vázquez, A. M. García-Deibe, J Sanmartín-Matalobos, J. M. Herrera and E. Colacio, *Inorg. Chem.*, 2017, **56**, 5646-5656. (b) M. Fondo, J. Corredoira-Vázquez, A.

Herrera-Lanzós, A. M. García-Deibe, J Sanmartín-Matalobos, J. M. Herrera, E. Colacio and C. Nuñez, *Dalton Trans*., 2017, **46**, 17000–17009. (c) M. Fondo, J. Corredoira-Vázquez, A. M. García-Deibe, S. Gómez-Coca, E. Ruiz and J. Sanmartín-Matalobos, *Dalton Trans*., 2020, **49**, 8389-8401.

20. M. Fondo, J. Corredoira-Vázquez, A. M. García-Deibe, J Sanmartín-Matalobos, M. Amoza, A. M. P. Botas, R. A. S. Ferreira, L. D. Carlos and E. Colacio, *Inorg. Chem. Front*. 2020, **7**, 3019-3029.

21. M. Fondo, J. Corredoira-Vázquez, A. M. García-Deibe, J Sanmartín-Matalobos, S. Gómez-Coca and E. Ruiz, Colacio, *Inorg. Chem. Front*., 2021, **8**, 2532–2541.

22. L.-W. Yang, S. Liu, E. Wong, S. J. Rettig and C. Orvig, *Inorg. Chem*., 1995, **34**, 2164-2178.

23. M. Fondo, A. M. García-Deibe, M. Corbella, M. R. Bermejo and J. Sanmartín, *Dalton Trans*. 2005, 3785-3794.

24. (a) G. M. Sheldrick, *SADABS, Area-Detector Absorption Correction*; Siemens Industrial Automation, Inc.: Madison, WI, 2001. (b) G. M. Sheldrick, *TWINABS* 2012/1. Bruker, Madison, Wisconsin, USA, 2012.

25. (a) G. M. Sheldrick, *Acta Cryst.* 2015, **A71**, 3-8. (b) G. M. Sheldrick, *Acta Cryst.* 2015, **C71**, 3–8.

26. I. Fdez. Galván, M. Vacher, A. Alavi, C. Angeli, F. Aquilante, J. Autschbach, J. J. Bao, S. I. Bokarev, N. A. Bogdanov, R. K. Carlson, L. F. Chibotaru, J. Creutzberg, N. Dattani, M. G. Delcey, S. S. Dong, A. Dreuw, L. Freitag, L. M. Frutos, L. Gagliardi, F. Gendron, A. Giussani, L. González, G. Grell, M. Guo, C. E. Hoyer, M. Johansson, S. Keller, S. Knecht, G. Kovačević, E. Källman, G. Li Manni, M. Lundberg, Y. Ma, S. Mai, J. P. Malhado, P. A. Malmqvist, P. Marquetand, S. A. Mewes, J. Norell, M. Olivucci, M. Oppel, Q. M. Phung, K. Pierloot, F. Plasser, M. Reiher, A. M. Sand, I. Schapiro, P. Sharma, C. J. Stein, L. K. Sørensen, D. G. Truhlar, M. Ugandi, L. Ungur, A. Valentini, S. Vancoillie, V. Veryazov, O. Weser, T. A. Wesołowski, P-O. Widmark, S. Wouters, A. Zech, J. P. Zobel, R. Lindh and R. *J. Chem. Theor. Comput.*, 2019, **15**, 5925-5964.

27. B. O. Roos, R. Lindh, P-Å. Malmqvist, V. Veryazov and P-O. Widmark, *J. Phys. Chem. A*, 2004, **108**, 2851-2858.

28. B. O. Roos, R. Lindh, P-Å. Malmqvist, V. Veryazov and P-O-Widmark, *J. Phys. Chem. A.*, 2005, **109**, 6575–6579.

29. L. Ungur and L. F. Chibotaru, *Chem. Eur. J.*, 2017, 23, 3708–3718.

30. A. Abragam and B. Bleaney, *Electron Paramagnetic Resonance of Transition Ions*, Oxford University Press, 1970.

31. P. G. Jones, *Acta Crystallogr., Sect. A*, 1986, **42**, 57.

32. J. Sanmartín, A. M. García-Deibe, M. R. Bermejo, F. Novio, D. Navarro and M. Fondo, *Eur. J. Inorg. Chem*., 2003, 3905-3913.

33. (a) M. Llunell, D. Casanova, J. Cirera, J. M. Bofill, P. Alemany, S. Alvarez, M. Pinsky and D. D. Avnir, SHAPE v1.1b, Barcelona, 2005; (b) A. Ruiz-Martínez, D. Casanova and S. Alvarez, *Chem. Eur. J.*, 2008, **14**, 1291–1303; (c) M. Llunell, D. Casanova, J. Cirera, P. Alemany and S. Alvarez, SHAPE: Program for the stereochemical analysis of molecular fragments by means of continuous shape measures and associated tools; University of Barcelona, Barcelona, Spain, 2010.

34. A. Raya-Barón, I. Oyarzabal, F. M. Arrabal-Campos, J. M. Seco, A. Rodríguez-Diéguez and I. Fernández, *Inorg. Chem*., 2017, **56**, 8768–8775.

35. J-L. Liu, Y-C. Chen and M-L. Tong, *Chem. Soc. Rev*., 2018, **47**, 2431—2453.

36. Z-H. Li, Y-Q. Zhai, W-P. Chen, Q-C. Luo, T. Han and Y-Z. Zheng, *Inorg. Chem. Front*., 2020, **7**, 4367-4376.

37. X-W. Liu, Z. Wu, J-T. Chen, L. Li, P. Chen, and W-B. Sun, *Inorg. Chem. Front*., 2020, **7**, 1229-1238.

38. L. Zhang, H. Ma, Z-Q. Wang, Y-M. Tian, Y-Q. Zhang and W-B. Sun, *J. Mol. Struct*., 2019, **1175**, 686-697.

39. G. Cucinotta, M. Perfetti, J. Luzon, M. Etienne, P-E. Car, A. Caneschi, G. Calvez, K. Bernot and R. Sessoli, *Angew. Chem.*, 2012, **124**, 1638-1642.

40. D. Reta and N. F. Chilton, *Phys. Chem. Chem. Phys.*, 2019, 21, 23567—23575.